Optimization of Two-Dimensional Multiple-Quantum MAS NMR Experiments for $I = {}^3/_2$ Nuclei on a Moderate-Field Spectrometer

Minoru Hanaya

Department of Chemistry, Faculty of Science, Tokyo Institute of Technology, Ookayama, Meguro-ku, Tokyo 152, Japan

Robin K. Harris*

Department of Chemistry, Durham University, South Road, Durham DH1 3LE, England

Received: March 28, 1997; In Final Form: June 30, 1997[⊗]

To test the efficiency of the two-dimensional multiple-quantum magic-angle spinning (2D MQMAS) method for half-integer quadrupolar nuclei on a moderate-field spectrometer, the experiments were performed for $RbNO_3$, $Na_5P_3O_{10}$, and $Na_2C_2O_4$ at a static magnetic-field strength of 4.7 T by using a two-pulse sequence and a three-pulse *z*-filter sequence. The procedure for data-processing has been carefully considered. In both types of experiment, high resolution was obtained in the isotropic (ν'_1) dimension of the 2D spectra, allowing a clear distinction for the crystallographically different sites of ^{87}Rb and ^{23}Na in the samples even with the moderate-field spectrometer. A large improvement was observed in the lineshapes of triple-quantum-filtered single-quantum MAS cross sections by use of the three-pulse *z*-filter sequence, and a further improvement was achieved by applying rotor-synchronized acquisition in the t_1 domain. A new approach to lineshape fitting for the cross sections, which uses the information in the isotropic dimension as a constraint for the NMR parameters, was introduced, and the validity of this method was demonstrated. The MQMAS method was also applied to NaCl crystallites, and the resulting 2D spectrum indicated the possible use of such crystallites as a chemical shift reference sample in practice, not only for the MAS (ν_2) dimension but also for the isotropic (ν'_1) dimension. The effects on resolution in the isotropic dimension of changes in the applied magnetic field are discussed.

1. Introduction

The demonstration of Frydman and Harwood that a two-dimensional multiple-quantum magic-angle spinning method can result in isotropic NMR spectra for half-integer quadrupolar nuclei[1,2] has brought exciting new possibilities for solid-state NMR. The advantage of this new method is its easy implementation through the use of an ordinary MAS probe, in contrast to the DOR or DAS methods, because the MQMAS method involves only sample rotation at the magic angle. The 2D MQMAS method has begun to be applied for a number of compounds involving the quadrupolar nuclei ^{17}O, ^{23}Na, ^{27}Al, ^{55}Mn and ^{87}Rb.[2−10] Modifications of the pulse sequences and of data acquisition and processing procedures have been pursued vigorously[5,6,11−13] because of the high potential of this new method.

In the theory of the 2D MQMAS method a quadrupolar Hamiltonian is treated as a perturbation to a dominant Zeeman Hamiltonian, and thus 2D MQMAS NMR benefits from a high-field scenario where the Larmor frequency is large compared to the quadrupolar frequencies.[2] In practice, so far, the 2D MQMAS experiments have been performed under relatively high static field strengths of more than 7 T, usually with high excitation radio frequency (rf) pulse strengths and high sample spinning rates. However, it is valuable to check the efficiency of the 2D MQMAS method on a moderate-field spectrometer. Moreover, the rf pulse strength and the sample spinning rate are rather limited in practice compared to the optimized conditions for the MQMAS experiment[14] by the capability of the spectrometer, including rf amplifiers and MAS probes.

Therefore, we tested the efficiency of the 2D MQMAS method on a moderate-field spectrometer for the $I = {}^3/_2$ nuclei ^{23}Na and ^{87}Rb by using a normal HX-type MAS probe. In this report, we compare the performance of the ordinary two-pulse sequence[2] and of the recently reported three-pulse *z*-filter sequence,[12] and we also discuss the effect of rotor-synchronized acquisition in the t_1 domain.[11] Furthermore, we define the data-processing procedure precisely, and we propose a new approach to line-shape fitting for the cross section in the MAS dimension (corresponding to the first ν_2 dimension) of 2D MQMAS spectra by using the information in the isotropic dimension (corresponding to the second ν'_1 dimension), simultaneously.

2. Experimental Section

In this paper, $RbNO_3$ (Fluka, >99.0%), $Na_5P_3O_{10}$ (Aldrich, >85%), $Na_2C_2O_4$ (Aldrich, >99.99%), and NaCl (BDH, >99.5%) were used without further purification as test samples for 2D MQMAS experiments. NMR spectra were recorded at 4.7 T static magnetic field strength (corresponding to 65.48 MHz for ^{87}Rb and 52.94 MHz for ^{23}Na) on a Chemagnetics CMX200 spectrometer. The spectrometer was fitted with a Chemagnetics HX probehead using 7.5 mm o.d. rotors. The measurements were performed using a rotor spinning rate ν_{rot} of 6 kHz (5 kHz spinning rate was used only for the measurement of NaCl crystallites). The ^{79}Br signal of KBr was employed to calibrate the magic angle, and the ^{87}Rb and ^{23}Na spectra were referenced with respect to an aqueous $RbNO_3$ solution (1 mol dm^{-3}) and an aqueous NaCl solution (1 mol dm^{-3}), respectively.

In the 2D MQMAS experiment using the two-pulse sequence, the rf nutation rate of the pulse was set to 83.3 kHz for both

* To whom correspondence should be addressed. Fax: +44-191-386-1127. E-mail: r.k.harris@duham.ac.uk.

[⊗] Abstract published in *Advance ACS Abstracts,* August 15, 1997.

S1089-5639(97)01108-0 CCC: $14.00

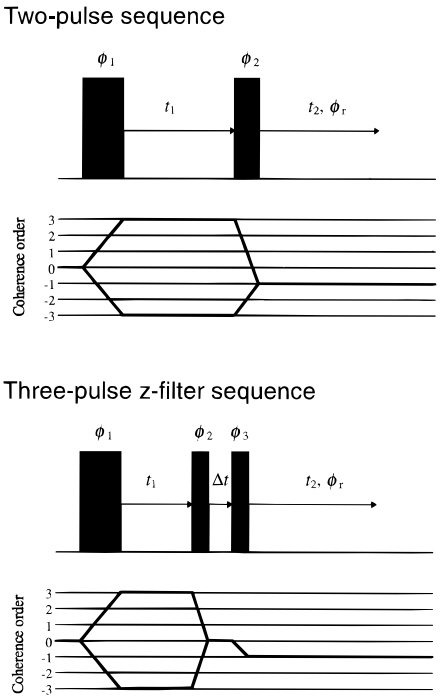

Figure 1. Radio frequency pulse sequence used for the two-dimensional MQMAS experiments in this study.

^{87}Rb and ^{23}Na nuclei[15] by monitoring the signal intensity of the reference solutions. In the case of the three-pulse *z*-filter sequence, the rf nutation rates of the first and second pulses were set to 83.3 kHz, while that for the third pulse was set to 41.7 and 12.5 kHz for the ^{87}Rb and ^{23}Na nuclei, respectively. The delay between the last two pulses was kept as 10 μs. The numbers of the acquired transients were between 144 and 432 with the relaxation delays between 0.5 and 2 s.

Rotor-synchronized data acquisition in the t_1 domain was performed by setting the time increment in t_1 as $1/\nu_{rot}$; thus, the dwell time in the t_1 domain was set to 166.67 μs in the experiment with $\nu_{rot} = 6$ kHz, for example.

3. Data Acquisition and Manipulation

3.1. Pulse Sequences. In this work, we used both the two-pulse sequence[2,4,5] and the three-pulse *z*-filter sequence[12] to compare their practical performances. The hypercomplex method[16] was applied for data collection in both cases in order to produce pure absorption-mode line shapes in the two-dimensional spectra. The pulse sequences are shown in Figure 1.

In the two-pulse sequence, two different phase cycles were used; one was composed of six phases for the first pulse, for selecting triple-quantum coherence (which is the same as reported previously[5]), and the other was composed of not only the six phases for the first pulse but also six in the second pulse, for the selection of coherence transfer to -1 from triple-quantum coherence (in order to avoid undesirable effects from the incomplete relaxation of the magnetization during the relaxation delay). The latter phase-cycling was constructed as in Table 1. This generates a signal $s_x(t_1,t_2)$ having cosine modulation with respect to the t_1-evolution time. The sine-modulated signal during t_1, $s_y(t_1,t_2)$, is obtained by a 30° (=90°/$|p|$, where p is the coherence order in the evolution period, here $|p| = 3$) phase shift in the first pulse.

In the three-pulse *z*-filter sequence, the phase cycling was composed of six phases in the first pulse, for selecting triple-quantum coherence, and four in the third pulse, for the selection of coherence transfer to -1 from zero-quantum coherence with

TABLE 1: Phase Cycling for the Two-Pulse Sequence

ϕ_1	0°	60°	120°	180°	240°	300°
ϕ_2	0°	0°	0°	0°	0°	0°
	60°	60°	60°	60°	60°	60°
	120°	120°	120°	120°	120°	120°
	180°	180°	180°	180°	180°	180°
	240°	240°	240°	240°	240°	240°
	300°	300°	300°	300°	300°	300°
ϕ_r	0°	180°	0°	180°	0°	180°
	240°	60°	240°	60°	240°	60°
	120°	300°	120°	300°	120°	300°
	0°	180°	0°	180°	0°	180°
	240°	60°	240°	60°	240°	60°
	120°	300°	120°	300°	120°	300°

TABLE 2: Phase Cycling for the Three-Pulse Sequence

ϕ_1	0°	60°	120°	180°	240°	300°
ϕ_2	0°					
ϕ_3	0°	0°	0°	0°	0°	0°
	90°	90°	90°	90°	90°	90°
	180°	180°	180°	180°	180°	180°
	270°	270°	270°	270°	270°	270°
ϕ_r	0°	180°	0°	180°	0°	180°
	90°	270°	90°	270°	90°	270°
	180°	0°	180°	0°	180°	0°
	270°	90°	270°	90°	270°	90°

suppression of the transfer from triple-quantum coherence,[17] keeping the second-pulse coherence selection as free. This leads to the phase cycle for $s_x(t_1,t_2)$ as in Table 2. Corresponding $s_y(t_1,t_2)$ signals are generated by incrementing the first-pulse phase by 30°.

In this work, all the three phase cycles were used in combination with CYCLOPS[18] to minimize phase and amplitude mis-setting of the receiver.

3.2. Data Processing. When considering the $I_z = -m \leftrightarrow I_z = +m$ ($m \geq 0$) transition, the evolution phase ψ_1 in the 2D MQMAS method during t_1 can be written as

$$\psi_1 = \nu_1 t_1$$

$$= \mp\left[2m\nu^{CS} + C_0^I(m)\nu_0{}^Q - \frac{7}{18}C_4^I(m)\nu_4{}^Q(\theta,\varphi)\right]t_1$$

for a coherence of order $p = \pm 2m$, where ν^{CS} corresponds to an isotropic chemical-shift frequency.[2] $C_0^I(m)$ and $C_4^I(m)$ are zero- and fourth-rank coefficients defined as

$$C_0^I(m) = 2m[I(I+1) - 3m^2]$$

$$C_4^I(m) = 2m[18I(I+1) - 34m^2 - 5]$$

while $\nu_0{}^Q$ is the isotropic quadrupolar shift, which depends on the quadrupolar coupling constant $\chi = (e^2qQ/h)$, the asymmetry parameter η and the Larmor frequency ν_L as

$$\nu_0{}^Q = -\frac{\chi^2(3+\eta^2)}{10\nu_L[2I(2I-1)]^2}$$

The variable $\nu_4{}^Q(\theta,\varphi)$ is a fourth-rank angular-dependent frequency, where θ and φ are angles defining the orientation of the external field B_0 with the principal axis system of the quadrupolar tensor. Thus ψ_1 is calculated for triple-quantum coherence of $p = \pm 3$ in the $I = {}^3/_2$ case as

$$\psi_1 = \nu_1 t_1$$

$$= \mp\left[3\nu^{CS} - 9\nu_0{}^Q + \frac{49}{3}\nu_4{}^Q(\theta,\varphi)\right]t_1.$$

SCHEME 1

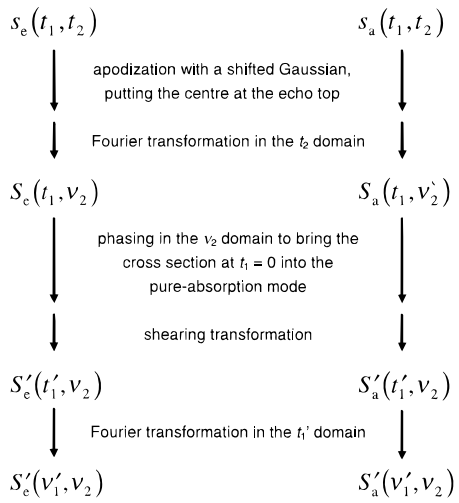

On the other hand, the evolution phase ψ_2 during t_2 can be calculated for $p = -1$ as

$$\psi_2 = \nu_2 t_2$$

$$= \left[\nu^{CS} + C_0^I(^1/_2)\nu_0{}^Q - \frac{7}{18}C_4^I(^1/_2)\nu_4{}^Q(\theta,\varphi)\right]t_2$$

$$= [\nu^{CS} + 3\nu_0{}^Q - 21\nu_4{}^Q(\phi,\varphi)]t_2$$

The essence of the MQMAS approach is allowing magnetization to evolve during consecutive times t_1 and t_2 under the influence of two different coherence orders ($p_1 = \pm 2m_1$ and $p_2 = \pm 2m_2$) to counterbalance the term involving $\nu_4{}^Q(\theta,\varphi)$, which is responsible for the observed line broadening. This second-order averaging is achieved by fulfilling

$$\mp C_4^I(m_1)t_1 \mp C_4^I(m_2)t_2 = 0$$

which is performed by selecting $p_1 = -3$ and $p_2 = -1$ for the $I = {}^3/_2$ case, resulting in refocusing to an isotropic echo at $t_2 = (7/9)t_1$ in the t_2 evolution time.

This coherence pathway ($p = 0 \rightarrow -3 \rightarrow -1$) is defined as an antiecho pathway, and that of $p = 0 \rightarrow +3 \rightarrow -1$ as an echo pathway. The echo and antiecho signals, $s_e(t_1,t_2)$ and $s_a(t_1,t_2)$, are produced from $s_x(t_1,t_2)$ and $s_y(t_1,t_2)$ as follows:

$$s_e(t_1,t_2) = s_x(t_1,t_2) - is_y(t_1,t_2)$$

$$s_a(t_1,t_2) = s_x(t_1,t_2) + is_y(t_1,t_2)$$

In this study, the data processing was performed for $s_e(t_1,t_2)$ and $s_a(t_1,t_2)$ separately as shown in Scheme 1 and reported in the literature.[5] Finally, the two sets of processed data were combined as

$$S(\nu'_1,\nu_2) = S_e(-\nu'_1,\nu_2) + S'_a(\nu'_1,\nu_2)$$

to obtain the absorption-mode line shape by cancellation of the dispersion part.

The main difficulty in data processing for the MQMAS method is the requirement for a shearing transformation to obtain untilted 2D spectra, which allow the observation of isotropic spectra by simple projection.[19] This transformation is performed by multiplying $S_e(t_1,\nu_2)$ and $S_a(t_1,\nu_2)$ by $e^{-i\phi(t_1,\nu_2)}$ and $e^{i\phi(t_1,\nu_2)}$, respectively, where $\phi(t_1,\nu_2)$ is defined as $k\nu_2 t_1$ (with $k = {}^7/_9$ in the $I = {}^3/_2$ case), and ν_2 is the frequency referenced to the carrier frequency ν_c, not the frequency difference from the chemical-shift reference frequency ν_0.[20] This shearing transformation is the equivalent of first-order phasing for a 1D spectrum obtained with quadrature detection.

In practice, multiplication of $S(t_1,\nu_2)$ by $e^{i\phi(t_1,\nu_2)}$ is performed in most commercial spectrometers by the combination of first-order phasing with $(2\pi t_1 k/\Delta t_2)$ and zeroth-order phasing with $(-\pi t_1 k/\Delta t_2)$, where Δt_2 is the dwell time in the t_2 dimension. However, the frequency in a spectrum conventionally runs from high to low, and opposite phase shifts have to be applied for some spectrometers in the multiplication by $e^{i\phi(t_1,\nu_2)}$.

After the process of shearing, there is a difference in data treatment between various papers; one[2] treats t_1 as t'_1 and others[5,7,11] treat $(1 + k)t_1$ as t'_1, which would cause some confusion in the evaluation of processed 2D spectra, especially as regards the meaning of the ν'_1 value at the spectral peak. If the loss of the FID signal before the echo top in the t_2 domain, which causes a poor signal-to-noise ratio, is ignored, the shearing corresponds to delayed acquisition of the FID signal,[21] i.e., if acquisition in the t_2 domain is performed from the echo top, the resulting 2D spectra have the same shape as sheared 2D spectra in which the FID signal was acquired just after the final rf pulse. This means that the time shift in the t_2 domain corresponds to the shearing, and the shearing procedure of the originally observed signal $s(t_1,t_2)$ into the sheared signal $s'(t'_1,t'_2)$ can be formulated in mathematical terms as follows:

$$s(t_1,t_2) = s'(t'_1,t'_2) = s'(\mathbf{At})$$

with

$$\boldsymbol{t} = \begin{pmatrix} t_1 \\ t_2 \end{pmatrix}$$

$$\boldsymbol{A} = \begin{pmatrix} 1 & 0 \\ -k & 1 \end{pmatrix}$$

which brings $t'_1 = t_1$ and $t'_2 = t_2 - kt_1$, and thus

$$\boldsymbol{A}^{-1} = \begin{pmatrix} 1 & 0 \\ k & 1 \end{pmatrix}$$

and $|\boldsymbol{A}| = 1$. According to the similarity theorem of Fourier transformation,[16] we can derive a relationship which connects the two corresponding spectra:

$$S(\nu_1,\nu_2) = \frac{1}{|\boldsymbol{A}|}S'(\tilde{\nu}\boldsymbol{A}^{-1})$$

$$= S'(\nu_1 + k\nu_2,\nu_2)$$

$$\tilde{\nu} = (\nu_1,\nu_2)$$

This clearly shows there is no need for the multiplication of t_1 by $(1 + k)$, and thus ν'_1 by $1/(1 + k)$, after shearing. Actually, when the data were processed without the multiplication, the spinning sidebands in the ν'_1 dimension appear with the correct frequency separation of ν_{rot}.

The origin of this multiplication by $(1 + k)$ seems to lie in the data processing for spin-echo correlation spectroscopy (SECSY) in which the delayed acquisition method was used and the time delay before acquisition was included in t_1.[22] To get the same scale in the ν_1 dimension of foldover-corrected correlated spectroscopy (FOCSY), in which the same pulse sequence with SECSY was used, but the data acquisition was started immediately after the final rf pulse and the data were processed with shearing (foldover correction), the multiplication of ν_1 by $1/(1 + k)$ was needed.[16,22] In the MQMAS method, t_1 is defined as the evolution time for multiple-quantum coherence, and t_2 as that for single-quantum coherence. Thus there is no

reason to apply multiplication by $(1 + k)$ for t_1 after shearing, which could cause undesirable confusion in data treatment.

When ν_c is set to ν_0, the ν'_1 value at the spectral peak after shearing is calculated for the case of $I = {}^3/_2$ nuclei as

$$\begin{aligned}\nu'_1 &= \nu_1 + k\nu_2 \\ &= (3\nu^{CS} - 9\nu_0{}^Q) + k(\nu^{CS} + 3\nu_0{}^Q) \\ &= (3 + k)\nu^{CS} - (9 - 3k)\nu_0{}^Q\end{aligned}$$

with $k = {}^7/_9$. If ν_c is set to a different frequency from ν_0, the observed ν'_1 value at the peak, $\nu'_1{}^{obs}$, is calculated as

$$\begin{aligned}\nu'_1{}^{obs} &= (3 + k)(\nu_L - \nu_c) - (9 - 3k)\nu_0{}^Q \\ &= (3 + k)(\nu_L - \nu_0) - (9 - 3k)\nu_0{}^Q - (3 + k)(\nu_c - \nu_0) \\ &= \nu'_1 - (3 + k)(\nu_c - \nu_0)\end{aligned}$$

This means that the carrier frequency offset from the chemical shift reference frequency appears $(3 + k)$ times larger in the ν'_1 domain than in the ν_2 domain, and careful calculation is needed to bring the spectral peak to the middle of the 2D spectra in the ν'_1 dimension, which is usually required for the application of rotor-synchronized acquisition in the t_1 domain.

3.3. Line-Shape Simulation and Parameter Fitting. In the case of the central $I_z = +{}^1/_2 \leftrightarrow I_z = -{}^1/_2$ transition for $I = {}^3/_2$ nuclei, the resonance frequency for a single crystal under magic-angle spinning with infinite rotation frequency is determined as follows:

$$\nu = \nu_L - \frac{3 + \eta^2}{120}\frac{\chi^2}{\nu_L} - \frac{1}{480}\frac{\chi^2}{\nu_L}f$$

where

$$f = \frac{35}{4}(3 - \eta\cos 2\alpha)^2 \sin^4\beta - 5(18 + \eta^2 - 9\eta\cos 2\alpha)\sin^2\beta + 18 + \eta^2$$

and α and β determine the orientation of the spinner with respect to the principal axis system of the electric-field-gradient tensor characterized by the quadrupolar coupling constant χ and asymmetry parameter η.[23,24] It is thus possible to build the frequency histogram, i.e., line shape, by calculating ν and summing the intensity for the range of $0 \le \alpha < 2\pi$ and $0 \le \cos\beta \le 1$. The usual line-shape calculation for the spectra broadened by the second-order quadrupolar interaction has been performed in this manner.

On the other hand, in the 2D MQMAS method the 2D spectra have not only the information in the ν_2 dimension but also that in the ν'_1 dimension. In the case of $I = {}^3/_2$ nuclei, ν'_1 is related to ν^{CS} $(=\nu_L - \nu_0)$, χ, and η as

$$\begin{aligned}\nu'_1 &= \frac{34\nu^{CS} - 60\nu_0{}^Q}{9} \\ &= \frac{34(\nu_L - \nu_0)}{9} + \frac{\chi^2(3 + \eta^2)}{54\nu_L}\end{aligned}$$

because

$$\nu_0{}^Q = -\frac{\chi^2(3 + \eta^2)}{360\nu_L}$$

and thus ν_L can be calculated directly from χ, η, ν_0, and the ν'_1 value at the peak.[25] Therefore, if the ν'_1 value is put as a constant in the line-shape fitting, the calculation is performed by changing only the χ and η parameters, resulting in a more accurate estimation of NMR parameters.[26] In this paper, we used this new approach in the line-shape fitting procedure. Errors in the parameters obtained from the fitting procedure were estimated by changing the ν'_1 values by an appropriate amount, taking account of standard deviations in the results.

4. Results and Discussion

Figure 2 shows ^{87}Rb two-dimensional MQMAS NMR spectra for $RbNO_3$ obtained with two different pulse sequences and different measurement conditions. Figure 2a is the result of the two-pulse sequence, both pulse durations being set to correspond to 180° pulse angles, (b) is that of the two-pulse sequence with the first pulse of 270° and the second pulse of 90°, (c) is that of the three-pulse *z*-filter sequence with the first pulse of 240°, the second pulse of 90° and the third softened pulse of 100°, and (d) is that of three-pulse *z*-filter sequence under the same pulse conditions as (c) but with rotor-synchronized acquisition in the t_1 domain. All of these four 2D spectra clearly show the existence of three different sites of Rb in $RbNO_3$, and no significant differences were observed in spectral resolution depending on the pulse sequence and measurement conditions. As shown in the projections in the ν'_1 dimension, the relative intensities of the signals from the three different sites were not greatly affected by the changes of the acquisition procedures.

However, the line shapes of the cross sections for the peaks in the ν'_1 dimension, which are shown in Figure 3,[27] depend significantly on the pulse sequence. In Figure 3, (a)−(d) correspond to those in Figure 2, while (e) is the best-fitted simulated spectrum for the line shape of (d) by the nonlinear least-squares method with the fitting procedure mentioned in the previous section. For all the three sites, the line shapes in the ν_2 dimension were significantly improved, from the theoretical point of view,[23] by applying the *z*-filtering method. This improvement is most clearly observed in the line shape of site 1; the peak around −35 ppm was observed as a shoulder in (a) and (b), which are the results of the two-pulse sequence, and appeared as a distinct peak in (c) by the three-pulse *z*-filter sequence. This is considered to be the result of a correct counterbalance of the echo and antiecho signal intensities performed by the *z*-filtering method. The line shape was improved further by rotor-synchronized acquisition in the t_1 domain, which produces a hypothetical infinite spinning rate in the t_1 domain as shown in (d). The ^{83}Rb NMR parameters obtained by the lineshape fitting are listed in Table 3.

The triple-quantum excitation is anisotropic and depends on the orientation of crystallites, and this anisotropy is larger for slower spinning rates.[2] It has been also reported that the line shape of the center band in 1D MAS spectra of quadrupolar nuclei which are broadened by the second-order quadrupolar interaction is affected by the spinning rate,[28] and that finite spinning rates may cause distortion of the line shape from that expected under infinite spinning rate in the 2D MQMAS spectra as well. However, the experimentally obtained line shapes of the cross sections from the three-pulse *z*-filter sequence with rotor-synchronized acquisition resemble closely the simulated ones (Figure 3d,e), and the NMR parameters obtained correspond well to the reported values (Table 3). These results show the validity of the line-shape fitting under the assumption of a single-quantum transition for MAS with an infinite spinning rate even for the medium-field spectrometer with a rather limited spinning rate.

According to the theoretical calculation, echo and antiecho signal intensities can be counterbalanced by setting the second-

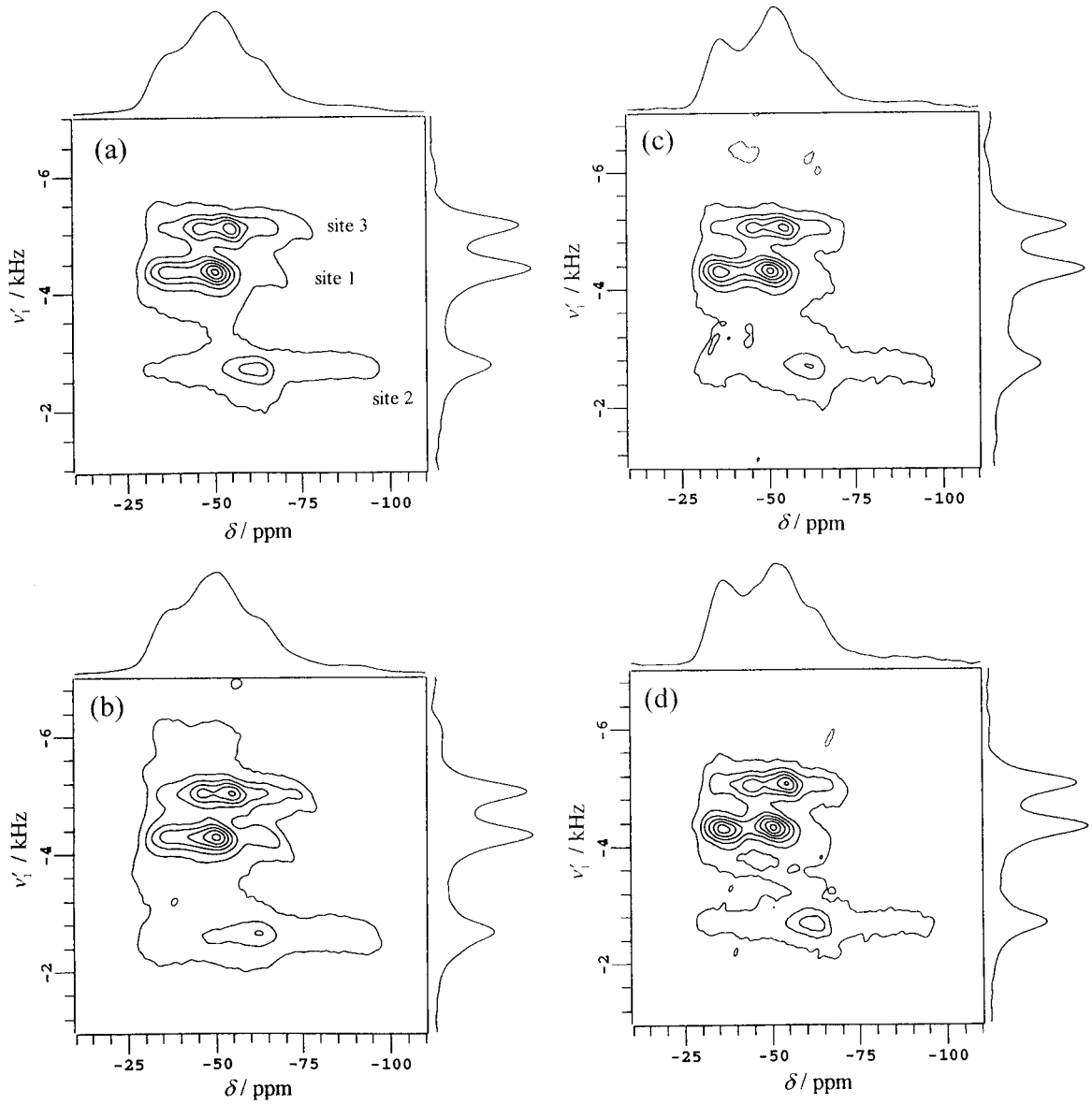

Figure 2. Two-dimensional triple-quantum ^{87}Rb MAS spectra of $RbNO_3$ crystallites, in which the contour lines are drawn every 15%, starting at a level of 5% and ending at 95% of the maximum in the respective spectrum: (a) the result of the two-pulse sequence with both pulse durations set to correspond to a "liquid-state" 180° pulse; (b) the result of the two-pulse sequence with the durations set to correspond to a "liquid-state" 270° and a "liquid-state" 90° for the first and second pulses, respectively; (c) the result of the three-pulse *z*-filter sequence with the durations set to corresponding to a "liquid-state" 240°, 90°, and 100° for the first, second, and third pulses, respectively; (d) the result of the three-pulse *z*-filter sequence under the same pulse conditions as (c) but with rotor-synchronized acquisition in the ν'_1 dimension.

TABLE 3. ^{87}Rb and ^{23}Na NMR Parameters for $RbNO_3$ and Sodium Salts Obtained by Fitting to the Triple-Quantum-Filtered Single-Quantum MAS Cross-Section Line Shapes in 2D MQMAS Spectra[a]

compound	site	ν'_1/Hz[b]	δ^{cs}/ppm (lit. value)[c]	χ/MHz (lit. value)	η (lit. value)
$RbNO_3$[d]	Rb(1)	-4310 ± 50	-27.5 ± 0.2 (-27.4)	1.69 ± 0.01 (1.68)	0.25 ± 0.01 (0.2)
	Rb(2)	-2690 ± 50	-28.9 ± 0.3 (-28.5)	2.01 ± 0.01 (1.94)	0.94 ± 0.01 (1.0)
	Rb(3)	-5040 ± 50	-31.4 ± 0.2 (-31.3)	1.71 ± 0.01 (1.72)	0.55 ± 0.01 (0.5)
$Na_5P_3O_{10}$[e]	Na(1)	2630 ± 50	0.2 ± 0.9 (-4.5)	1.36 ± 0.02 (1.4)	$1.00 - 0.06$ (0.9)
	Na(2)	3690 ± 80	7.2 ± 0.4 (-14.5)	1.32 ± 0.01 (1.75)	0.81 ± 0.02 (0.8)
$Na_2C_2O_4$[e]	Na(1)	8090 ± 50	1.0 ± 0.2 (1.0)	2.52 ± 0.01 (2.6)	0.75 ± 0.01 (0.7)

[a] Errors are reported on the bases of the accuracy estimated for experimental observations and of the standard deviations in the lineshape fittings. [b] Directly observed frequency shift of the peak in the isotropic dimension of the two-dimensional spectrum. [c] True isotropic chemical shift, free of second-order quadrupolar effects, obtained from fitting the cross sections in the MAS dimension subject to the constraint: $9\nu'_1 = 34\nu^{CS} - 60\nu_0^Q$, where $\nu_0^Q = -(3 + \eta^2)\chi^2/360\nu_L$. [d] Literature values are from ref 5. [e] Literature values are from ref 2.

pulse duration to 90° in the two-pulse sequence for $I = {}^3/_2$ nuclei.[14] However, the change of the second-pulse duration from 180° to 90° did not improve the line shape in the cross sections, as shown in Figure 3a,b. This result shows the difficulty of setting the second-pulse duration in order to cancel the dispersion in the final 2D spectra with the two-pulse sequence, and suggests the higher performance in practice of the three-pulse *z*-filter sequence even in the triple-quantum coherence for the $I = {}^3/_2$ case.

The higher performance of the three-pulse *z*-filter sequence was also observed for ^{23}Na MQMAS NMR of $Na_5P_3O_{10}$. Figure 4 shows the 2D spectra of $Na_5P_3O_{10}$ for the two-pulse sequence (a) and for the three-pulse *z*-filter sequence with rotor-synchronized acquisition in the t_1 domain (b). In both the

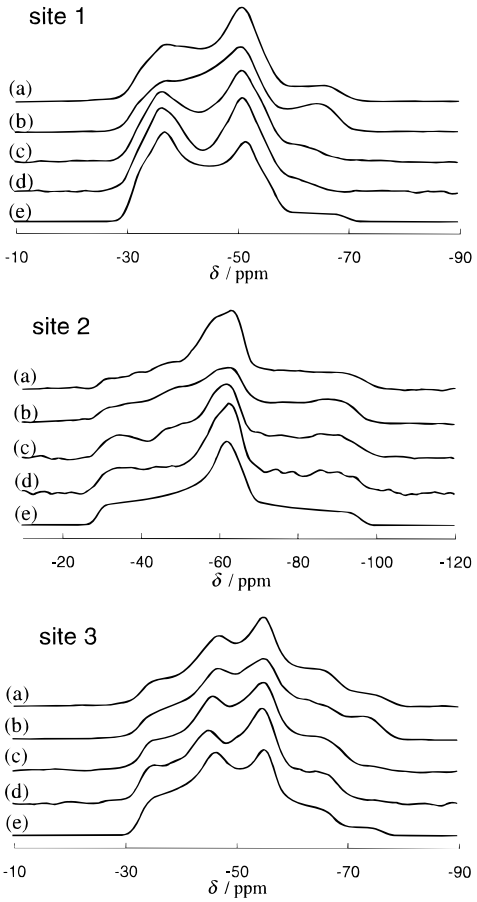

Figure 3. Triple-quantum-filtered single-quantum MAS cross sections obtained from 2D MQMAS spectra of $RbNO_3$ at the peaks of the spectrum in the isotropic (ν'_1) dimension. The cross sections were produced by summing adjacent slices which have intensities of more than 80% of the maximum: the notation (a)−(d) corresponds to that of Figure 2; (e) best-fitted simulation for the line shape of (d).

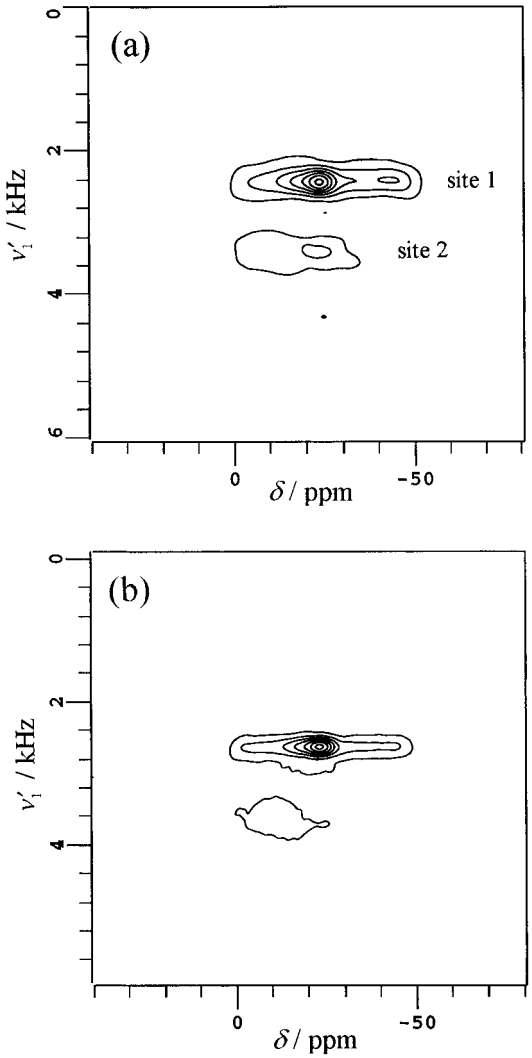

Figure 4. Two-dimensional triple-quantum ^{23}Na MAS spectra of $Na_5P_3O_{10}$ crystallites, in which the contour lines are drawn every 15%, starting at a level of 5% and ending at 95% of the maximum in the respective spectrum: (a) the result of the two-pulse sequence with pulse durations set to correspond to a "liquid-state" 270° and a "liquid-state" 90° for the first and second pulses, respectively; (b) the result of the three-pulse *z*-filter sequence with the durations set to correspond to a "liquid-state" 240°, 90°, and 40° for the first, second, and third pulses, respectively, and with rotor-synchronized acquisition in the ν'_1 dimension.

spectra, the existence of two distinct sites for Na is clearly observed. However, the line shapes in the cross sections at the peaks in the ν'_1 dimension are rather distorted for the two-pulse sequence measurement, as shown in Figure 5a. These are significantly improved by the use of *z*-filtering and rotor-synchronized acquisition (Figure 5b). The improvement of the line shapes allowed reasonable fitting by line-shape simulation (Figure 5c). The NMR parameters obtained for ^{23}Na are also listed in Table 3.[29]

The MQMAS method was originally proposed to get high resolution in the second (ν'_1) dimension in 2D spectra and has been shown to give high performance in distinguishing different sites for half-integer quadrupolar nuclei as reported in several papers[2−5,7−10,26] and as shown in this paper. However, the MQMAS method has advantages over the 1D MAS method even when the sample has only one site for the quadrupolar nuclei in question. One of these involves the use of the ν'_1 value at the peak in 2D spectra, which allows a more accurate estimation of NMR parameters by line-shape fitting, as mentioned in the previous section, and the other is the elimination of the overlapping of spinning sidebands (ssb) with the center band in 1D MAS spectra. Figure 6a shows the 2D MQMAS spectra for $Na_2C_2O_4$ obtained by the three-pulse *z*-filter sequence with rotor-synchronized acquisition in the t_1 domain. This sample has only one site for Na, with a relatively large quadrupolar coupling constant. In this case, the limitation of the spinning rate brought overlapping of ssb's in the ν_2 dimension, as shown in the projection of the 2D spectrum onto the ν_2 axis, which almost corresponds to the 1D MAS spectrum, resulting in serious line-shape distortion. However, the ssb's in the ν_2 dimension were brought to different frequencies in the ν'_1 dimension from that of the center band after the shearing transformation, corresponding to their frequency difference in ν_2 from the center band.[30] Thus the cross sections were free from the overlapping of ssb's, as shown in Figure 6b, and simple line-shape fitting assuming an infinite spinning rate is possible in practice, as shown in the figure. The estimated parameters are listed in Table 3. They correspond well to the parameters reported previously, showing the validity of the simple line-shape fitting, as was the case for $RbNO_3$.

On the other hand, it seems valuable to check the MQMAS 2D spectrum of NaCl powdered crystal as a chemical shift reference sample, not only for the ν_2 dimension but also for the ν'_1 dimension, to obtain more accurate values in the ν'_1 dimension. In theory, the excitation of triple-quantum coherence is impossible for $\chi = 0$ nuclei which is the case of ^{23}Na nuclei in a perfect crystal of NaCl. However, NaCl crystals generally possess substantial numbers of lattice defects, which cause nonzero χ values for nearby Na nuclei, and an MQMAS signal is therefore expected for NaCl crystallites. Figure 7 shows the result of measurement by the two-pulse sequence for NaCl. The

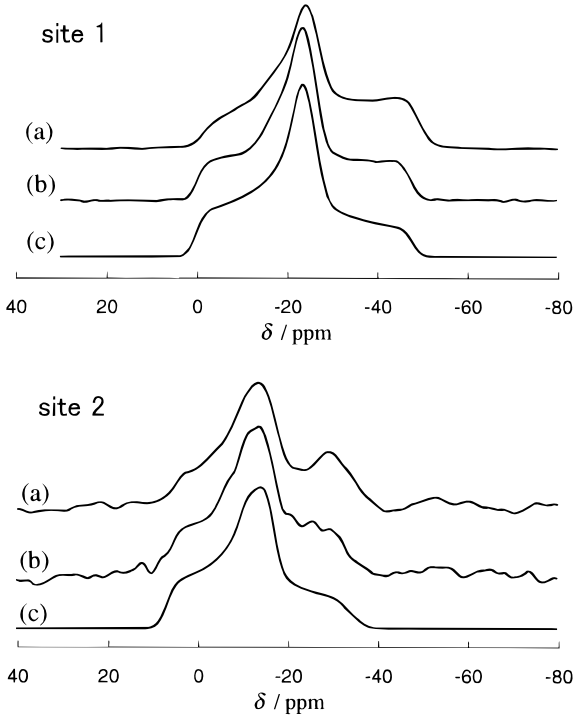

Figure 5. Triple-quantum-filtered single-quantum MAS cross sections obtained from 2D MQMAS spectra of $Na_5P_3O_{10}$ at the peaks in the spectrum projected onto the isotropic (ν'_1) axis, where the cross sections were produced by summing adjacent slices which have intensities of more than 70% of the maximum: the notation (a) and (b) corresponds to that of Figure 4; (c) best-fitted simulation for the line shape of (b).

peak position was observed as 7.1 ppm (corresponding to 377 Hz) in the ν_2 dimension and 1450 Hz in the ν'_1 dimension. The values of ν^{CS} and χ were directly calculated from the ν'_1 and ν_2 positions according to the relations $\nu'_1 = (34\nu^{CS} - 60\nu_0{}^Q)/9$ and an averaged frequency $\langle\nu_2\rangle = \nu^{CS} + 3\nu_0{}^Q$ to be 381 Hz (corresponding to 7.2 ppm) and 0.1 MHz, respectively, with the assumptions $\langle\nu_2\rangle = \nu_2$ and $\eta = 0$. However, the χ value (which will be some sort of average over the relevant sites) is quite small and the observed ν'_1 and ν_2 values are very close to the theoretical expectation of $\nu'_1 = (3 + k)\nu_2$, where $k = {}^7/_9$, for the $\chi = 0$ case, showing the possibility of using NaCl crystallites to provide a chemical shift reference sample also in the ν'_1 dimension.[31] Since the data processing procedure of the 2D MQMAS method is rather more complicated than those of normal COSY-type 2D methods, it would be useful to test whether such data processing is performed in a correct way or not by checking the position of the peak arising from NaCl crystallites.

As long as the static magnetic field is strong enough to treat a quadrupolar Hamiltonian as a perturbation to a dominant Zeeman Hamiltonian, the lineshape of a cross section in the MAS dimension of 2D MQMAS spectra will not be affected by a variation of the field strength, although the line width will be reduced with increase of the field strength. Such line-width narrowing results in a better signal-to-noise ratio of the spectra, but it brings some loss of precise information from the line shape.

On the other hand, the spectral resolution in the isotropic ν'_1 dimension will show rather complicated behavior with the change of field strength. Since the ν'_1 value at the peak is calculated as

$$\nu'_1 = \frac{34\nu^{CS} - 60\nu_0{}^Q}{9}$$

in the 2D MQMAS spectra of $I = {}^3/_2$ nuclei, the difference of

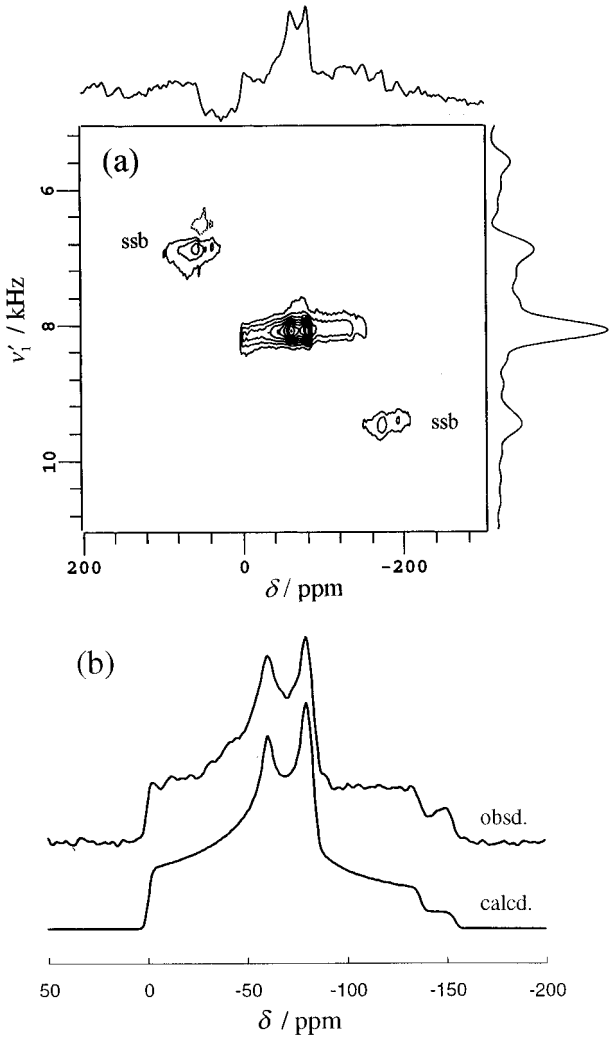

Figure 6. Results of the two-dimensional triple-quantum ^{23}Na MAS experiment for $Na_2C_2O_4$ from the three-pulse *z*-filter sequence with pulse durations set to correspond to a "liquid-state" 210°, 90°, and 40° pulse angles for the first, second, and third pulses, respectively, and with rotor-synchronized acquisition in the ν'_1 dimension: (a) 2D MQMAS spectrum in which the contour lines are drawn every 10%, starting at a level of 10% and ending at 90% of the maximum in the spectrum; (b) triple-quantum-filtered single-quantum MAS cross section of the peak in the spectrum in the isotropic (ν'_1) dimension, along with the best-fitted simulation, where the cross section was produced by summing adjacent slices which have intensities of more than 70% of the maximum.

ν'_1 between different sites, $\Delta\nu'_1$, depends on the magnitudes of the differences in both ν^{CS} and $\nu_0{}^Q$. For two different sites A and B, $\Delta\nu'_1$ is expressed as

$$\Delta\nu'_1 = \frac{34(\nu_A^{CS} - \nu_B^{CS}) - 60(\nu_{0A}^Q - \nu_{0B}^Q)}{9}$$

While $|\nu_A^{CS} - \nu_B^{CS}|$ is proportional to the field strength, $|\nu_{0A}^Q - \nu_{0B}^Q|$ is in inverse proportion to the field strength. Therefore, $|\Delta\nu'_1|$ has a minimum for a field strength where

$$34|\nu_A^{CS} - \nu_B^{CS}| = 60|\nu_{0A}^Q - \nu_{0B}^Q|$$

If

$$34|\nu_A^{CS} - \nu_B^{CS}| > 60|\nu_{0A}^Q - \nu_{0B}^Q|$$

then the $|\Delta\nu'_1|$ value increases with increasing field strength, so that the spectral resolution becomes better in the isotropic dimension, and vice versa.

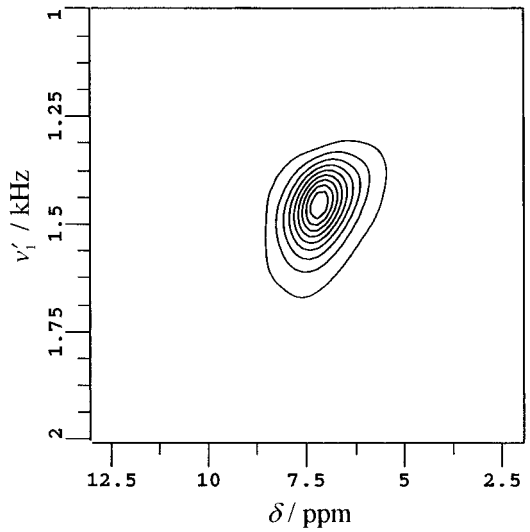

Figure 7. Two-dimensional triple-quantum ^{23}Na MAS spectrum of NaCl crystallites, produced by the two-pulse sequence with the pulse durations set to correspond to a "liquid-state" 270° and a "liquid-state" 90° for the first and second pulses, respectively. The contour lines are drawn every 10%, starting at a level of 10% and ending at 90% of the maximum in the spectrum.

In the case of sites 1 and 2 in $RbNO_3$, for example, $34|\nu_1^{CS} - \nu_2^{CS}| < 60|\nu_{01}^{Q} - \nu_{02}^{Q}|$ in the present study at field strength 4.7 T (see the values in Table 3). Therefore, the obtained value, $|\Delta\nu'_1| = 1620$ Hz, in our experiment is expected to become smaller in a higher-field measurement. On the other hand, for the case of sites 1 and 3, $34|\nu_1^{CS} - \nu_3^{CS}| > 60|\nu_{01}^{Q} - \nu_{03}^{Q}|$ so that $|\Delta\nu'_1| = 730$ Hz is expected to become larger in higher fields. These changes in $|\Delta\nu'_1|$ are evident from comparisons of our data with the literature, where values of $|\Delta\nu'_1|$ obtained using a 7 T field[5] were evaluated to be 750 and 1410 Hz for the former and the latter cases, respectively.

5. Conclusion

We have shown that the 2D MQMAS method, which has been used with high-field spectrometers, has high potential even using a moderate-field (4.7 T) spectrometer. The 2D spectra obtained by the two-pulse sequence and the three-pulse *z*-filter sequence show no significant difference in resolution in the isotropic (ν'_1) dimension. However, the line shape of cross sections in the MAS (ν_2) dimension is significantly improved by using the three-pulse *z*-filter sequence, and further improvement in the line shape is realized by the application of rotor-synchronized acquisition in the t_1 domain.

The results show higher performance for the three-pulse *z*-filter sequence than for the "ordinary" two-pulse sequence. In practice, optimization of the pulse duration is much easier in the three-pulse *z*-filter sequence, and efficient shortening of the experimental time is brought about by rotor-synchronized acquisition.

In general, spectra obtained on lower-field spectrometers have higher sensitivity to the values of the anisotropic interactions. This is also true in 2D MQMAS spectra, and accurate NMR parameters are obtainable from spectra given by a moderate-field spectrometer, and a possibility of resolution enhancement in the isotropic (ν'_1) dimension is shown to occur in some cases on lowering the field.

Acknowledgment. We thank the U.K. EPSRC for research grants GR/H96096 and GR/J97557. M.H. is grateful to the Ministry of Education, Science, Culture, and Sports of Japan for financial support. We also thank G. McGeorge and A. Nordon for assistance with spectrometer operation.

References and Notes

(1) Frydman, L.; Harwood, J. S. *J. Am. Chem. Soc.* **1995**, *117*, 5367.
(2) Medek, A.; Harwood, J. S.; Frydman, L. *J. Am. Chem. Soc.* **1995**, *117*, 12779.
(3) Fernandez, C.; Amoureux, J. P. *Chem. Phys. Lett.* **1995**, *242*, 449.
(4) Fernandez, C.; Amoureux, J. P. *Solid State NMR* **1996**, *5*, 315.
(5) Massiot, D.; Touzo, B.; Trumeau, D.; Coutures, J. P.; Virlet, J.; Florian, P.; Grandinetti, P. J. *Solid State NMR* **1996**, *6*, 73.
(6) Brown, S. P.; Heyes, S. J.; Wimperis, S. *J. Magn. Reson.* **1996**, *A119*, 280.
(7) Wu, G.; Rovnyank, D.; Sun, B.; Griffin, R. G. *Chem. Phys. Lett.* **1996**, *249*, 210.
(8) Hanna, J. V.; Smith, M. E.; Whitfield, H. J. *J. Am. Chem. Soc.* **1996**, *118*, 5772.
(9) Baltisberger, J. H.; Xu, Z.; Stebbins, J. F.; Wang, S. H.; Pines, A. *J. Am. Chem. Soc.* **1996**, *118*, 7209.
(10) Kraus, H.; Prins, R.; Kentgens, A. P. M. *J. Phys. Chem.* **1996**, *100*, 16336.
(11) Massiot, D. *J. Magn. Reson.* **1996**, *A122*, 240.
(12) Amoureux, J. P.; Fernandez, C.; Steuernagel, S. *J. Magn. Reson.* **1996**, *A123*, 116.
(13) Wu, G.; Rovnyank, D.; Griffin, R. G. *J. Am. Chem. Soc.* **1996**, *118*, 9326.
(14) Amoureux, J. P.; Fernandez, C.; Frydman, L. *Chem. Phys. Lett.* **1996**, *259*, 347.
(15) In the experiment on NaCl crystallites, the rf nutation rate of the pulse was set to 50.0 kHz.
(16) Ernst, R. R.; Bodenhausen, G.; Wokaun, A. *Principles of Nuclear Magnetic Resonance in One and Two Dimensions*; Oxford: Oxford, 1987; Chapter 6.
(17) This is the minimum phase cycling for $I = {}^3/_2$ nuclei, and 6-fold phase cycling is needed in the third pulse for the case of $I = {}^5/_2$ nuclei to suppress the coherence transfer to -1 from not only triple-quantum but also quintuple-quantum coherence.
(18) Hoult, D. I. *Prog. NMR Spectrosc.* **1978**, *12*, 41.
(19) Bax, A.; Griffey, R. H.; Hawkins, B. L. *J. Magn. Reson.* **1983**, *55*, 301.
(20) Although the shearing transformation can be performed with an arbitrary origin for ν_2, we defined ν_c as the origin for ν_2 in order to avoid unnecessary complexity, because the change of the origin affects the peak position in the ν'_1 dimension of 2D spectra.
(21) Schmidt-Rohr, K.; Spiess, H. W. *Multidinensional Solid-State NMR and Polymers*; Academic: New York, 1994; Chapter 4.
(22) Nagayama, K.; Kumar, A.; Wüthrich, K.; Ernst, R. R. *J. Magn. Reson.* **1980**, *40*, 321.
(23) Lefebvre, F.; Amoureux, J. P.; Fernandez, C.; Derouane, E. G. *J. Chem. Phys.* **1987**, *86*, 6070.
(24) Samoson, A. *Chem. Phys. Lett.* **1985**, *119*, 29.
(25) In practice, substitution of ν_L by ν_0 in the denominator of the second term is a sufficiently good approximation, which gives faster line-shape calculation under the constraint.
(26) Hanaya, M.; Harris, R. K. *Solid State NMR* **1997**, *8*, 147.
(27) In this paper, triple-quantum-filtered single-quantum MAS cross sections were produced by summing some slices around the corresponding peaks in the ν'_1 dimension in order to obtain better S/N spectra and to avoid rounding errors in the shearing treatment caused by the limited digital resolution.
(28) Massiot, D.; Kahn-Harari, A.; Michel, D.; Muller, D.; Taulelle, F. *Magn. Reson. Chem.* **1990**, *28*, S82.
(29) There is a large discrepancy between the present results and the reported values.[2] This seems to be due to a difference in hydration state or polymorphic form between the samples. (personal information from Dr. L. Frydman, University of Illinois and Dr. C. Jäger, University of Jena).
(30) In Figure 6a, the ssb's in the ν_2 dimension appear in the ν'_1 dimension folded back.
(31) The full width at the half-height of the peak in the ν'_1 dimension was about 100 Hz, which was determined by the relaxation time of the triple-quantum coherence, and the deviation of the observed ν'_1 value at the peak from the theoretically expected value is considered to be almost within the experimental error.